Optics & Laser Technology 181 (2025) 111863

Contents lists available at ScienceDirect

Optics and Laser Technology

journal homepage: www.elsevier.com/locate/optlastec

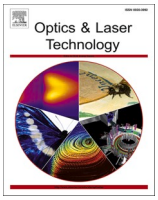

Full length article

Super-resolution lensless on-chip microscopy based on array illumination and scattering multiplexing with polystyrene microspheres layer

Yulong Li [a], Zhongrui Lin [a], Jianshe Ma [a], Chao Zuo [b,*], Ping Su [a,*]

[a] Tsinghua Shenzhen International Graduate School, Tsinghua University, Shenzhen 518055, China
[b] Smart Computational Imaging Laboratory (SCILab), Nanjing University of Science and Technology, Nanjing, Jiangsu Province 210094, China

ARTICLE INFO

Keywords:
Ptychography imaging
Scattering multiplexing
Super-resolution

ABSTRACT

The resolution of lensless on-chip microscopy is mainly limited by the pixel size of the image sensor. Many super-resolution techniques have emerged to solve the problem of insufficient imaging resolution. Most existing pixel super-resolution technologies rely on precise electric translation stage for hundreds of high-precision displacements, or on expensive tunable lasers to generate diffraction diversity. Conventional ptychography iterative engine (PIE) is considered an effective method for improving imaging resolution, but it is prone to oscillations in the early stage of iteration. In this paper, we propose a ptychography imaging technique based on scattering multiplexing, which involves coating the surface of the image sensor with a layer of polystyrene microspheres, and utilizing a 4 × 3 LED array to sequentially illuminate the sample. An innovative ptychography reconstruction algorithm based on dual amplitude gradient descent (DAGD) is designed for the reconstruction from the holograms, which effectively avoids the problems of slow convergence speed and obvious oscillation. Compared with other similar technologies, our system has no moving parts and uses inexpensive partially coherent light illumination. It only records 12 holograms and reaches the imaging resolution of 1.23 μm, which is 1.36 times pixel super-resolution compared with the pixel size of the sensor.

1. Introduction

Lensless microscopy is fundamentally a digital holography technique based on in-line holography, where photodetection sensor devices (such as CCD or CMOS) are utilized to replace the photogelatin plates for recording holograms. Subsequently, the holograms are stored in a computer, and the computer simulates the optical diffraction process to reconstruct the recorded objects. Lensless on-chip microscopy has attracted considerable attention in the field of biomedical sample detection due to its simplified optical design and the advantages of a large field of view and high resolution. Nonetheless, the resolution of conventional lensless on-chip microscopy is primarily limited by the coherence of the light source and the pixel size restriction of image sensors, preventing it from achieving the resolution capabilities of high numerical aperture optical microscopes.

In recent years, numerous techniques have been proposed to enhance the spatial resolution of on-chip microscopy by collecting more holograms with diffraction diversity. These include capturing multiple low-resolution holograms using multi-height [1-3], multi-wavelength [4-7], or multi-angular illumination [8-10] to synthesize high-resolution images. Some techniques employ precise displacement platforms to introduce sub-pixel shifts between different low-resolution images [11-15]. However, these methods often rely on high-precision electric displacement platforms, or expensive laser sources, resulting in increased device complexity and costs. Istrate et al. have proposed a multi-height phase reconstruction method, utilizing an electro-mechanical displacement stage to position the image sensor at 26 different height planes and record the sample's diffraction maps [2]. They added a small aperture behind the sample to confine the imaging area and employed a high dynamic range (HDR) algorithm to obtain the diffraction information within this illuminated region. This approach isolates interference from other areas of the sample, ensuring that the sensor records diffraction information solely from this minute region, thereby achieving higher imaging resolution. However, this method is significantly limited by its ability to record only a very small imaging area at a time, which negates the wide-field imaging advantage of lensless microscopy. Bishara et al. achieved sub-pixel image shifting by laterally translating the light source to 36 different positions using an electro-mechanical displacement stage. They rigorously improved the coherence of the light source by connecting an optical fiber and a

* Corresponding authors.
E-mail addresses: zuochao@njust.edu.cn (C. Zuo), su.ping@sz.tsinghua.edu.cn (P. Su).

https://doi.org/10.1016/j.optlastec.2024.111863
Received 14 June 2024; Received in revised form 28 August 2024; Accepted 24 September 2024
Available online 1 October 2024

monochromator to achieve higher imaging resolution [11]. They also introduced a novel system architecture using a monochromatic LED array as the light source, connected to 23 multimode fibers with an inner diameter of 105 μm, and added a narrowband filter at the fiber's end to enhance the light source's coherence, ultimately achieving good super-resolution effects [14]. However, the stringent alignment demands between the LED array and the fibers could compromise the system's reliability. Furthermore, the decoupling of the reconstruction process from the super-resolution algorithm hinders the effective removal of twin image interference, rendering the system less ideal for imaging dense samples.

Researchers have recently discovered that if a modulation layer is added before or after the sample, the modulation light carries more high-frequency information of the sample, which may result in higher resolution reconstruction if combined with a suitable iterative algorithm. Modulating the light source by a scattering layer, such as a mask [16-20] or a spatial light modulator (SLM) [21-25], can effectively enhance the resolution of lensless on-chip microscopy. Previous studies have unveiled the influence of the modulation feature size of the scattering layer on the resolution of reconstructed images [26]. Small modulation feature sizes contribute to the improvement of imaging quality. Most SLMs are manufactured using liquid crystal materials, and there is crosstalk between adjacent pixels, resulting in errors in the modulation process [21,22]. Consequently, the wavefront modulation by the SLM is coarse, which results in poor imaging quality [26]. To address this issue, Zheng et al. replaced the protective glass plate of the image sensor with a goat blood cell smear to modulate the diffracted light from the sample through secondary diffraction, and reconstructed the sample using the rPIE algorithm [27]. Goat blood cells are cost-effective and possess the smallest size among animal blood cells (2 ~ 3 μm). However, these cells exhibit varying absorption characteristics for different wavelengths of light, and the modulation size is still larger than the pixel size of the sensor. Another potential option to achieve finer modulation feature structures than blood cell layers is a disordered engineering surface with phase scattering and intensity absorption [28]. Nonetheless, sub-micron level precise surface structures incur high production costs.

The scattering layer usually has a fixed scattering pattern, so it is necessary to use a displacement device to generate relative displacement between the sample and collect more holograms with diffraction diversity. In 2022, Chang et al. moved the scattering layer to 150 positions to capture images [17]; In 2023, Zheng et al. moved the integrated sensor to 225 previously calibrated positions to capture images [26]. The above scattering multiplexing technologies both rely on high-precision displacement platforms to collect hundreds of diffraction intensity images in order to achieve super-resolution image reconstruction, which greatly increases the image acquisition time and computational complexity of the reconstruction process.

The forward and backward models in scattering multiplexing both involve two diffraction processes [17], making iteration more time-consuming. Ptychography iterative engine (PIE) is swiftly developing into a mainstream technique for phase imaging that uses iterative algorithms to reconstruct an image of a specimen from a series of diffraction patterns, and has been further extended to new versions such as ePIE and rPIE [29]. The transmittance function of the scattering layer and its position relative to the sample are often not known. It requires more computational resources and time to recover both the transmittance function of the scattering layer and the sample from an in-line hologram captured by an image sensor. Meanwhile, the iterative updating method between the scattering layer and the object makes the convergence process prone to oscillations, aggravating the instability of convergence.

This paper presents a lensless on-chip holography technique based on three-color LED array illumination and scattering multiplexing for wavefront modulation. This technique surmounts the limitations associated with image sensor pixel size, enabling sub-pixel super-resolution imaging. By coating the image sensor surface with a layer of polystyrene microspheres with diameters much smaller than the sensor pixel, a scattering layer is obtained. The array illumination induces relative displacement between the sample and the scattering plane, enabling different modulation patterns and providing richer constraints for the reconstruction process. The combination of illumination from multiple angles and multiple wavelengths, and scattering layers can generate more differences of diffraction information in fewer holograms, greatly enriches the diffraction diversity. To reconstruct super-resolution images, we propose a new ptychography reconstruction algorithm based on dual amplitude gradient descent (DAGD) that separates the updates of the scattering layer and the sample into two processes, achieving rapid reconstruction with fewer iterations and stable convergence. Compared with existing technologies, we use an inexpensive LED array for illumination, only requiring 12 holograms to be recorded without precise displacement or angle calibration. The reconstruction algorithm converges faster, breaking through the limitations of pixel size (1.67 μm) and achieving pixel super-resolution of 1.23 μm. This approach provides a low-cost and high-efficiency technical solution for portable lensless on-chip microscopy imaging systems.

2. Method

The holographic imaging system is comprised of an LED array, which consists of four sets of emitting chips arranging in 2 × 2 and with a spacing of 5 mm. Each set includes three chips emitting red, green, and blue light, with a chip spacing of 1 mm. The central wavelengths of these three chips are 625 nm, 525 nm, and 470 nm, each with a full width at half maximum (FWHM) of about 30 nm. This system also incorporates a sample, a scattering layer, and an image sensor. The schematic structure of the platform is shown in Fig. 1(a). To avoid resolution reduction caused by the increased diffraction distance due to the addition of an extra scattering plane inserted between the sample and the image sensor as in Ref. [17], we directly coat a layer of polystyrene microspheres (d = 0.5 μm, $n = 1.59$) on the protective glass surface of the image sensor. First, 0.5 μL polystyrene microsphere original solution is pipetted out using a pipette, and a certain amount of water is added for dilution. Subsequently, 0.5 μL diluted mixture is dispensed onto the glass surface using a pipette, and the solution is spread evenly across the surface using the edge of a coverslip. Finally, a heat gun is employed to evaporate the solution, allowing the microspheres to be immobilized on the glass surface, as depicted in Fig. 1(b). To prevent the liquid from being blown away by the heat gun, a cover glass can be placed over the sensor before heating. The concentration of the microsphere solution can be adjusted to modify the distribution density of microspheres on the glass slide as required.

2.1. Diffraction model

The distance between the LED array and the sample is set to 20 cm, while the distance from the sample to the image sensor is less than 1 mm, allowing the illumination light to be reasonably approximated as a plane wave. The maximum distance between the emitting chips is 8.6 mm (5 mm in the longitudinal direction and 7 mm in the lateral direction), and based on geometric relationships, the shifts of the holograms due to the translation of the light source are calculated to be less than 43 μm (approximately 26 pixels). The image sensor used has a resolution of 3872 × 2764 pixels, which is two orders of magnitude larger than the hologram shifts. Therefore, the illumination from each LED group can be approximated as vertical incidence, allowing us to describe the hologram generation through the classical angular spectrum diffraction model. Prior to sample placement, we captured the diffraction intensity patterns generated by the polystyrene microspheres layer using the image sensor:

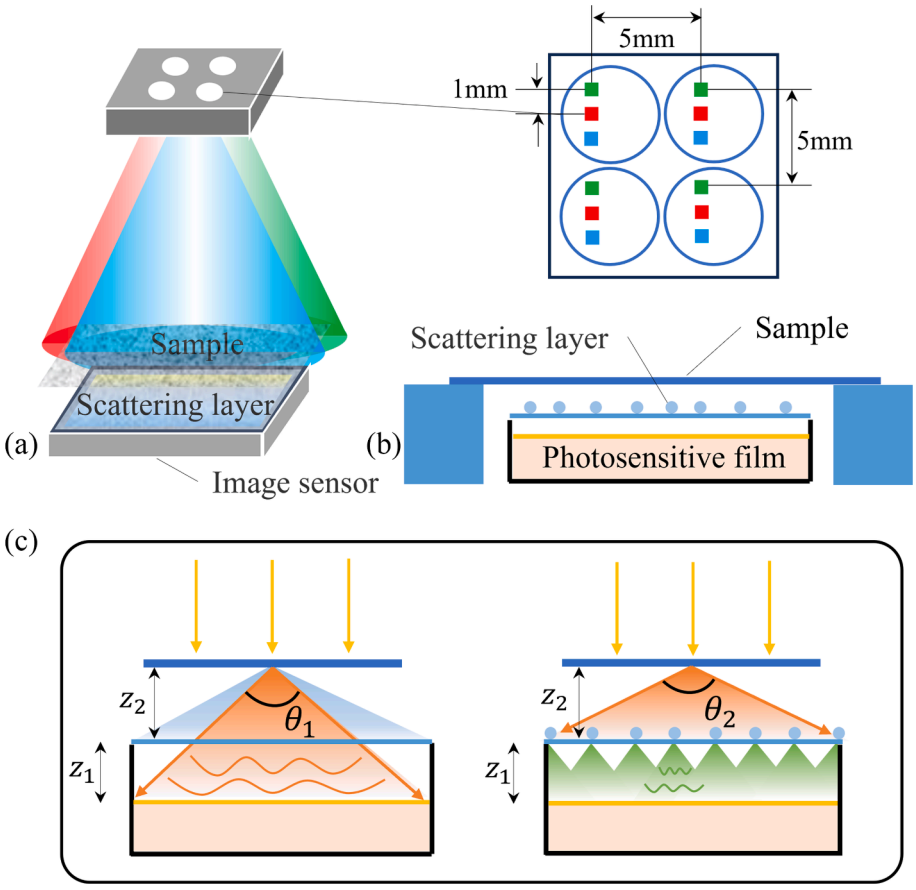

Fig. 1. Lensless on-chip microscopy based on LED array illumination and microsphere scattering layer. (a) is the system diagram, and (b) shows the recording system and the arrangement of emitting chips in LED array. (c) depicts the principle of the modulation by the scattering layer, where z_1 is the distance from the protective glass to the photosensitive film, z_2 is the distance from the sample to the protective glass. θ_1 is the diffraction angle range that can be captured by the sensor without modulation, and θ_2 is the diffraction angle range that can be captured by the sensor after modulation by the scattering layer.

$$u_0^k(x,y) = F^{-1}\left\{H(f_x,f_y,z_1,\lambda_s)\cdot F\{P(x,y)\}\right\} \tag{1}$$

$$H(f_x,f_y,z_1,\lambda_s) = \exp\left(\frac{j2\pi z_1}{\lambda_s}\sqrt{1-(\lambda_s f_x)^2-(\lambda_s f_y)^2}\right) \tag{2}$$

$$y_1^k = \left|u_0^k(x,y)\right|^2 + \eta \tag{3}$$

$P(x,y)$ represents the complex transmittance function of the scattering plane. k represents the illumination order of different LEDs in the array. (x,y) and $(f_x f_y)$ are coordinates in spatial and frequency domain, respectively. F and F^{-1} represent Fourier transform and inverse Fourier transform, respectively. H is the angular spectrum diffraction transfer function as in Eq. (2), and z_1 is the distance between the scattering plane and the sensor plane. $\lambda_{s=1,2,3}$ represent different incident light wavelengths, which are 625 nm, 525 nm, and 470 nm, respectively. The intrinsic noise of the sensor is represented by η, and y_1 is the recorded hologram of the scattering layer. Place the sample in front of the image sensor. The diffraction process of the object wave onto the scattering layer plane can be described as:

$$u_1^k(x,y) = F^{-1}\left\{H(f_x,f_y,z_2,\lambda_s)\cdot F\{O(x,y)\}\right\} \tag{4}$$

$O(x,y)$ represents the complex distribution of the sample. z_2 is the distance from the sample to the scattering plane. When the diffracted light reaches the scattering plane, it is modulated again by the polystyrene microspheres, followed by a second forward diffraction propagation, which can be described as:

$$u_2^k(x,y) = F^{-1}\left\{H(f_x,f_y,z_1,\lambda_s)\cdot F\left\{u_1^k(x,y)\cdot P(x-\Delta x_k, y-\Delta y_k)\right\}\right\} \tag{5}$$

During measurement, LED chips are sequentially illuminated in a clockwise direction, starting from the top right corner. In the k-th measurement, the relative displacement between the sample and the scattering layer changes due to the distance between the currently illuminated LED chip and the one illuminated in the previous measurement. The change in relative displacement compared to the first measurement is defined as $(\Delta x_k, \Delta y_k)$. The intensity distribution of the object wave collected by the image sensor after two diffractions y_2 can be described as:

$$y_2^k = \left|u_2^k(x,y)\right|^2 + \eta \tag{6}$$

Many studies suggest that sensors have two main impacts on the resolution of on chip holography: the limited capture range of sensors leads to the loss of high-frequency information of diffracted light, and the limited pixel spacing leads to under-sampling of holograms. The microsphere scattering layer used in this paper has a certain improvement effect on both of issues. First, the scattering layer converts the large diffraction angle of the object light wave into a smaller diffraction angle, allowing more high-frequency diffraction light to enter the capture range of the sensor. As depicted in Fig. 1(c), owing to the modulation effect of the scattering layer, the angular range within which the diffraction sub-waves of the specimen can be detected by the image sensor is extended from θ_1 to θ_2. Second, the scattered particles have a modulation feature size that is much smaller than the sensor pixel size, which provides fine wavefront modulation. The array light source

illumination produces relative displacement with the sample to change the modulation mode, providing more constraints for the iterative process in super-resolution reconstruction.

2.2. Reconstruction algorithm

We introduce a ptychography reconstruction algorithm based on dual amplitude gradient descent (DAGD) [30], which is inspired from the update process of rPIE [17,29]. We propose to use both the diffraction intensity maps of the scattering layer and the sample modulated by the scattering layer as dual constraints for reconstruction. During the iterative reconstruction process, we update the information of the scattering layer and the sample separately, and find the optimal solution of the objective function. Firstly, we update the distribution function of the scattering layer using the diffraction intensity maps of y_1:

$$\nabla f(u_0^k) = \left\| \sqrt{\boldsymbol{D}|u_0^k|^2} - \sqrt{y_1^k} \right\|_2 \tag{7}$$

$$P_t^{k+1} = P_t^k - \tau_t \mathbf{B}_1^k \{\mathbf{D}^*(\nabla f(u_0^k))\} \tag{8}$$

∇f is the amplitude error function. D is the down-sampling process. $D^\star$ is the up-sampling process. B_1 is the reverse diffraction process of z_1. t is the number of iterations. τ_t is the correction step size for the t-th iteration, and the initial value is usually set to 2. To ensure convergence speed and prevent missing the nearest neighbor interval of the optimal solution due to excessive step size, τ_t is set as an adaptive adjustment step size related to reconstruction error. Then we use the updated scattering layer and the diffraction intensity maps of y_2 to reconstruct the objective function:

$$\nabla f(u_2^k) = \left\| \sqrt{\boldsymbol{D}|u_2^k|^2} - \sqrt{y_2^k} \right\|_2 \tag{9}$$

$$O_t^{k+1} = O_t^k - \tau_t \mathbf{B}_2^k \left\{ \frac{\mathbf{B}_1^k \{\mathbf{D}^*(\nabla f(u_2^k))\} \cdot \mathrm{conj}(P_t^k)}{(1-\alpha)|P_t^k|^2 + \alpha \cdot \max(|P_t^k|^2)} \right\} \tag{10}$$

B_2 is the reverse diffraction process of z_2. α is a regulatory factor that adjusts the convergence stability for different brightness regions, and it is empirically set to 0.25. Eq. (10) is an innovative design based on the rPIE reconstruction algorithm. In each iteration of reconstruction process, the distribution function of the scattering layer is updated using the diffraction intensity map y_1 as shown in Eqs. (7) and (8), and then the object function is updated using the diffraction intensity map y_2 as shown in Eqs. (9) and (10). Compared to the conventional strategy of updating the sample and scattering layer [17,29], this approach introduces y_1 as a new iterative constraint, which can effectively eliminate the mutual coupling between the sample and scattering layer throughout the propagation process, making the updating process of the sample function have better convergence. Meanwhile, using two sets of diffraction intensity maps as constraints can make the reconstructed results closer to the true values. The complete algorithm flowchart is shown in Fig. 2.

3. Simulation results

A suspension of polystyrene microspheres is coated on the surface of the CMOS protective glass to form a microsphere scatter layer, whose distribution can be considered random. Therefore, a two-dimensional random matrix $M(x,y)$ is established to simulate the scattering layer, with each element of the matrix being either 0 or 1, where 0 represents a microsphere. Hence, the ratio of the count of all 0 elements to the total number of elements in the matrix is the distribution density of the microspheres. When there is no scattering layer, the matrix is an all-one matrix. Polystyrene microspheres have a certain degree of transparency and generate phase difference. In order to better simulate the distribution of microspheres in real scenes, we assume that the transmittance of the pixel points covered by scattering particles is 0.8 and the phase difference is $\pi/2$, so the complex function $P(x,y)$ of the scattering layer is set to:

$$P(x,y) = (0.8 + 0.2 \times M(x,y)) \times \exp\left(j\frac{\pi}{2} \times M(x,y)\right) \tag{11}$$

We perform simulations and compare the results by using the conventional method [5], the super-resolution reconstruction without a scattering layer and the proposed super-resolution reconstruction based on scattering multiplexing. The pixel size of the images and scattering layer is set to 1.1 μm, and the pixel size of the image sensor is set to 2.2 μm to simulate 2 × under-sampling. The distance z_1 between the scattering plane and the sensor, as well as the distance z_2 from the sample to the scattering plane were both set to 0.5 mm. The results in Fig. 3(a1) show that without using a scattering layer (i.e., the scattering layer matrix is an all-one matrix), the reconstruction obtained using the conventional method can only resolve group (7) element 1, whereas the reconstruction achieved using four illumination angles combined with a 2 × super-resolution algorithm can resolve group (7) element 4, as

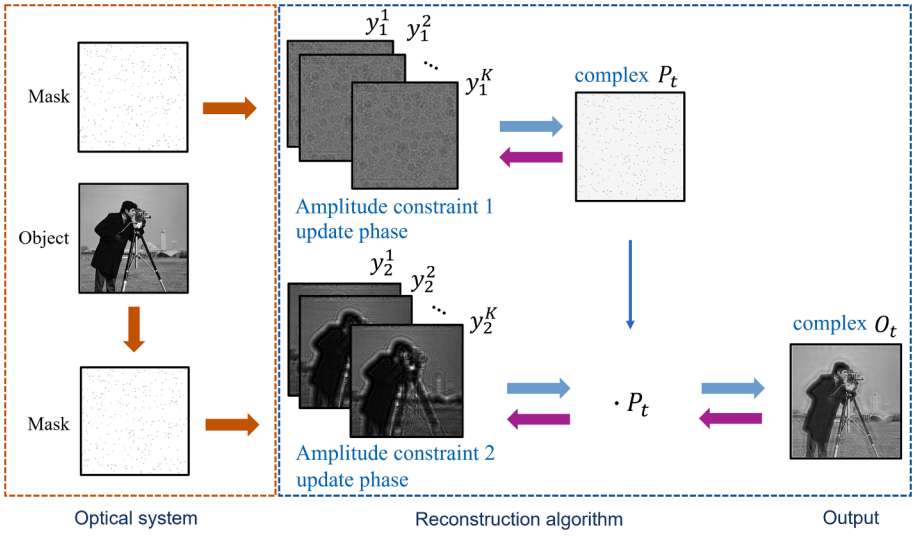

Fig. 2. Flowchart of the reconstruction algorithm based on the dual amplitude gradient descent strategy. Orange arrow represents the physical forward diffraction process, the blue arrow is the simulated backward diffraction process, and the purple arrow is the simulated forward diffraction process.

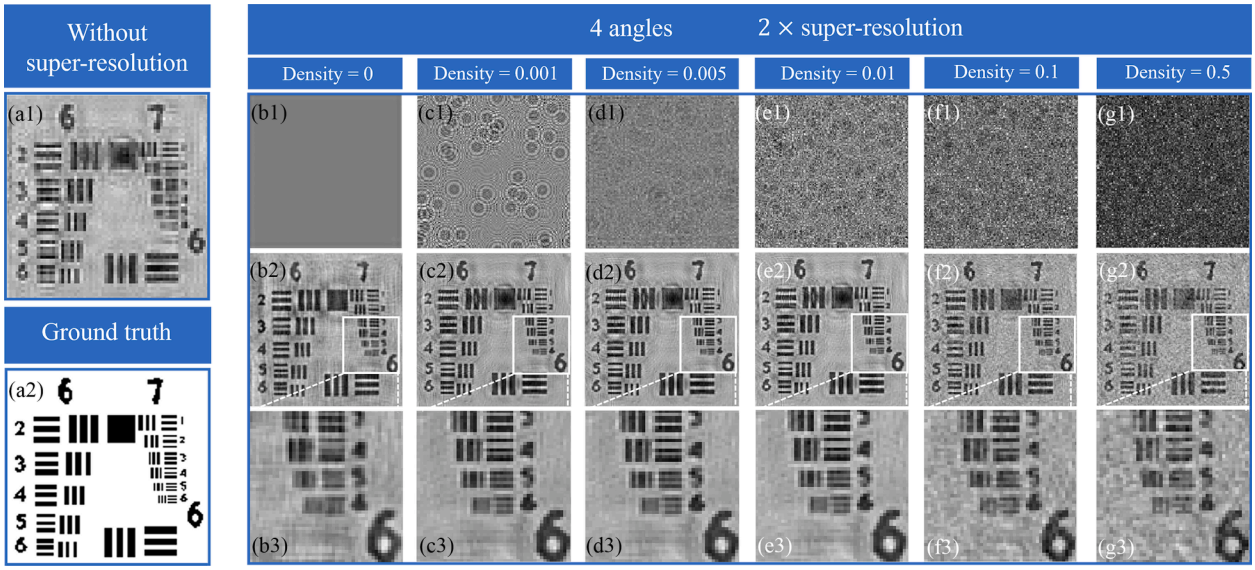

Fig. 3. The enhancement of resolution by the scattering layer and the impact of the scattering layer's distribution density on the reconstruction results. (a1) is the reconstruction result with no scattering layer and no super-resolution algorithm, and (a2) depicts the ground truth. (b1-g1) correspond to the diffraction intensity patterns for different densities of scattering layers. (b2-g2) are the reconstruction results for the respective densities of scattering layers, and (b3-g3) represent their locally magnified views.

shown in Fig. 3(b). Subsequently, we generate a scattering layer matrix with a distribution density of one-thousandth. Using the same four illumination angles and the proposed 2 × super-resolution reconstruction based on DAGD, the results indicate that the group (7) element 5 can be clearly resolved in Fig. 3(c). The comparison results indicate that the super-resolution reconstruction algorithm based on scattering multiplexing effectively enhances the imaging resolution of lensless on-chip microscopy systems.

Furthermore, we analyze the influence of the density of microspheres on the imaging resolution. As shown in Fig. 3(c), (d) and (e), the reconstructed images with a scattering modulation unit density of 0.001, 0.005 and 0.01 are clear, indicating that the density within this range would also yield good reconstruction results. This suggests that the modulation unit density has a broad range of variability, which consequently lowers the precision requirements for preparing and applying the polystyrene microsphere suspension in experimental settings. When the modulation unit density becomes extremely large, as evident from the reconstruction results shown in Fig. 3(f) and (g) for unit densities of 0.1 and 0.5, there is a significant degradation in imaging resolution. This is due to the highly overlapping diffraction gratings produced by the dense modulation units, which submerge the sample signal in noise. The results of comparative experiments indicate that there is no strict requirement for the density of modulation units in the scattering layer, but it is necessary to avoid overly dense arrangements that can produce larger amounts of noise.

The number of incident angles of the illumination light is also an important factor that affects the reconstruction performance. Within the range of small angle changes that are approximately along the vertical direction relative to the incidence, when there are more such vertical incidence angles, multiple relative displacements will occur between the

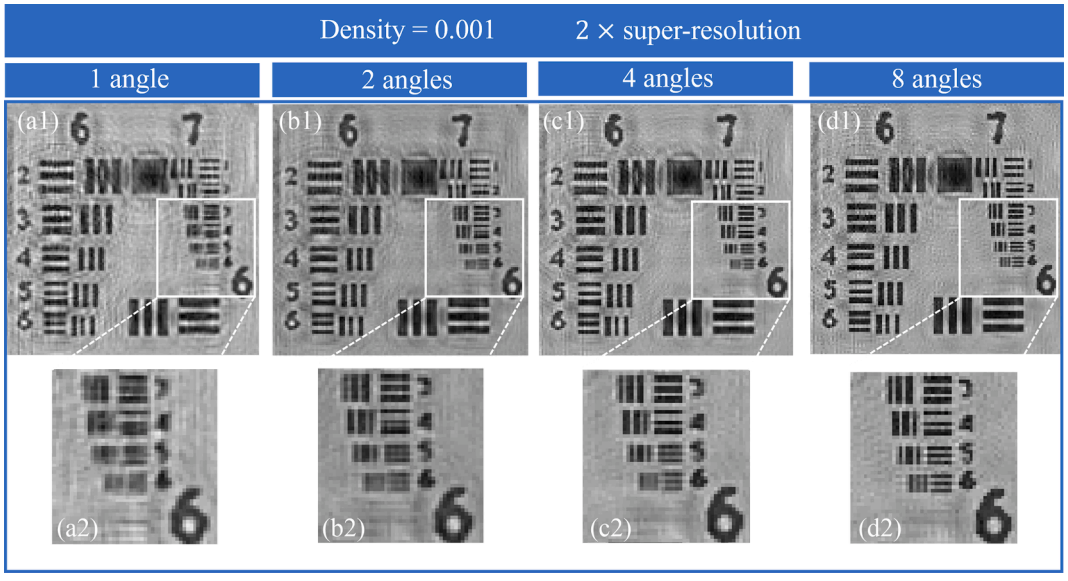

Fig. 4. Effect of number of incident angles on reconstruction results. (a1-d1) show the reconstruction results with different number of incident angles, and (a2-d2) correspond to the locally magnified views of them, respectively.

scattering layer and the sample, which can result in the formation of more modulation patterns. These relative displacements can be obtained through a simple image registration algorithm, obviating the need for any correction of the incident angle. We set the modulation unit density of the scattering layer to 0.001 and perform simulations with 1, 2, 4, and 8 incident angles. To verify that the reconstruction algorithm does not require precise angle information, the incident angles are set to random numbers near 90 degrees. The reconstruction results are shown in Fig. 4. When only one incident angle is used, the imaging resolution can only reach the group (7) element 3, as shown in Fig. 4(a). As the increasing of incident angle numbers, the reconstruction results approach the ground truth, as shown in Fig. 4(a)-(d). This demonstrates that the proposed multi-angle illumination module can provide angle information for the reconstruction process, which significantly enhances the imaging resolution of the system without the need for any calibration, thus improving experimental efficiency. Although we employed the multi-wavelength phase retrieval reconstruction method, which effectively suppresses the inherent twin image interference in in-line holography, the reconstructed results still exhibit some ringing artifacts.

4. Experiment

We conduct resolution testing by using a USAF 1951 resolution target. The CMOS senor is DMK 27AUJ003 (3872×2764, pixel size $=$ 1.67 μm) and its effective imaging area is $6.47 \times 4.62 mm^2$. The two diffraction distances can be rapidly and accurately obtained using the autofocus algorithm (NoG) [31], where the distance z_1 between the scattering layer and the sensor is 460 μm, and the distance z_2 from the sample to the scattering layer is 100 μm. We first sequentially light a group of RGB LED and capture three holograms with three colors. We reconstruct the amplitude distribution using the conventional multi-wavelengths reconstruction method [5], the results of which are shown in Fig. 5 (a). Due to the limitations of the image sensor pixel size, line patterns in group (8) and (9) are completely blurred and indistinguishable. The conventional method is only able to resolve group (7) element 6, with an imaging resolution of 2.2 μm.

Then, we sequentially light all of the 4×3 LED chips and capture the 12 holograms without a scattering layer for $4 \times$ super-resolution reconstruction. This operation successfully resolves group (8) element 3, corresponding to a resolution of 1.55 μm, as shown in Fig. 5 (b). Next, we apply a layer of polystyrene microsphere suspension (with a diameter $d = 0.5$ μm) on the protective glass surface of the image sensor and dry it with a hot air gun to fix the microspheres on the glass surface. We capture the diffracted intensity patterns of the scattering layer under the illumination of 12 LED chips for the proposed super-resolution algorithm based on DAGD for scattering multiplexing, one of which is shown in Fig. 5(c). We then place the sample on the scattering layer, and capture the 12 holograms under sequential illumination of the LED array. We perform the reconstruction by using the proposed super-resolution algorithm based on scattering multiplexing, which results an imaging resolution of 1.23 μm. Compared to the pixel size of the sensor, it achieves 1.36 times pixel super-resolution. This is a 1.79-fold improvement over the conventional method and a 20 % improvement over the results without a scattering layer.

To verify the impact of microsphere distribution density on the reconstruction results, we conduct a comparative experiment. By significantly increasing the density of the polystyrene microspheres in the experiment, the degree of overlap in the diffraction patterns of the scattering layer becomes extremely high, as shown in Fig. 5 (d1). This leads to the reduction of the resolution to 1.55 μm. Simultaneously, the contrast and clarity of the reconstructed image undergo severe degradation, causing some sample information to be submerged in the background noise, as shown in Fig. 5 (d2). It is worth noting that the vertical resolution displayed is slightly higher than the horizontal resolution in Fig. 5, which is due to the arrangement of the emitting chips in the LED array as shown in Fig. 1(b). The number of displacements of the

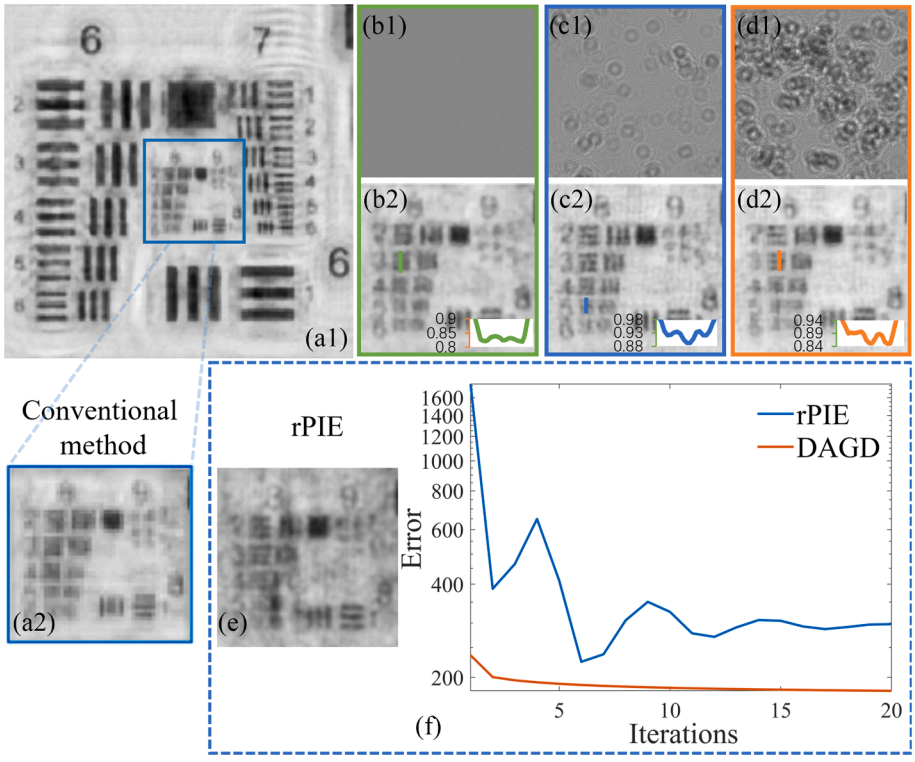

Fig. 5. Reconstruction results of a USAF 1951 resolution target obtained by different reconstruction algorithms. (a1) is the reconstruction result of the conventional method, and (a2) is the locally magnified view. (b1-d1) are diffraction intensity patterns for different densities of scattering layers. (b2-d2) are the reconstruction results for the respective densities of scattering layers. (e) is the reconstruction result of rPIE algorithm. (f) shows the error function curves of the rPIE algorithm and the proposed DAGD algorithm.

holograms in the vertical direction exceeds that in the horizontal direction.

We employed an up-sampling rate M = 4 in the recovery process and reconstructed a squared FOV with 650 by 650 pixels. At each iteration, the recovery process requires a memory size of ~103 MB, and the reconstruction time taking 5 iterations is 450.8 s (CPU: AMD Ryzen 7 5800H with Radeon Graphics, 3.20 GHz). The use of a high-performance GPU can significantly reduce the computation time. The comparative experiments have demonstrated the effectiveness of the super-resolution reconstruction algorithm based on DAGD, but care should be taken to avoid excessive overlap of diffraction patterns due to too high a distribution density of microspheres during the production of the scatterer layer, which could affect the quality of the reconstruction accuracy in turn.

We compare the proposed method with the conventional ptychography imaging algorithm rPIE [17,29]. The results show that although rPIE can ensure an overall decrease in error, there are relatively obvious oscillations in error during the iteration process. Analyzing the reasons, the wavefront diffracted from the sample into the scattering layer is updated interactively with the transmittance function of the scattering layer. This update way causes obvious oscillations in error, resulting in slow convergence speed. As shown in Fig. 5 (f), the proposed DAGD method outperforms rPIE in terms of convergence stability and reconstruction accuracy, as only one iteration is sufficient to bring the error to a very low level. We also compared the proposed method with two other ptychography imaging reconstruction algorithms, *BPD²O* [17] and *iAPG* [17,32]. Both methods utilize a laser as the light source and reconstruct holograms by moving a diffuser to 30 different positions and capturing holograms. They reported an imaging resolution of 1.23 μm with a sensor pitch 1.67 μm. In contrast, our method employs a cost-effective LED array as the light source and achieves the same imaging resolution by capturing only 12 holograms. In terms of algorithm complexity, our method incorporates an additional constraint with the hologram y_1 of the scattering layer, which entails one more gradient update step compared to the other two methods. However, since only 12 updates are required in each iteration, the reconstruction time per iteration is reduced. Under the same computational resource, the single iteration time of the proposed method is 90.1 s, whereas *BPD²O* and *iAPG* are 109.9 s and 117.6 s, respectively. Furthermore, due to the richer diffraction diversity of holograms, our method achieves satisfactory reconstruction quality with only five iterations, much less than the other two methods.

We conduct biological sample testing using a cross section of pine stems. Fig. 6(a) exhibits the full-field hologram of the section acquired by the image sensor, with the imaging fields of view (FOVs) for 4×, 10×, and 20 × microscope objectives labeled. Compared to traditional lens-based microscopy, the lensless on-chip microscopy system reveals a larger FOV. Fig. 6(b) shows the reconstruction results from the lensless on-chip system and the observation under a 20 × microscope objective for the same area of the section. The resolution test results mentioned previously indicate that the reported microscopy system is capable of achieving an imaging resolution of 1.23 μm, surpassing the resolution of a 10x microscope objective (NA = 0.2). Fig. 6(c) presents a comparison between the results of the conventional reconstruction algorithm and the proposed super-resolution reconstruction algorithm based on DAGD. The results indicate a significant improvement in image resolution, with the internal grid structure of the slice becoming clearer.

The technique still has room for improvement. For example, the insufficient coherence of the light source will affect the imaging resolution to some extent, including the temporal coherence determined by the light source bandwidth and the spatial coherence determined by the emission area [33]. The spectral bandwidth of the LEDs currently used is about 30 nm. The lateral size of the LEDs is 500 μm, and the distance from the LED array to the sample is set to 20 cm. The ratio of the lateral size of the light source to the distance from the light source to the sample

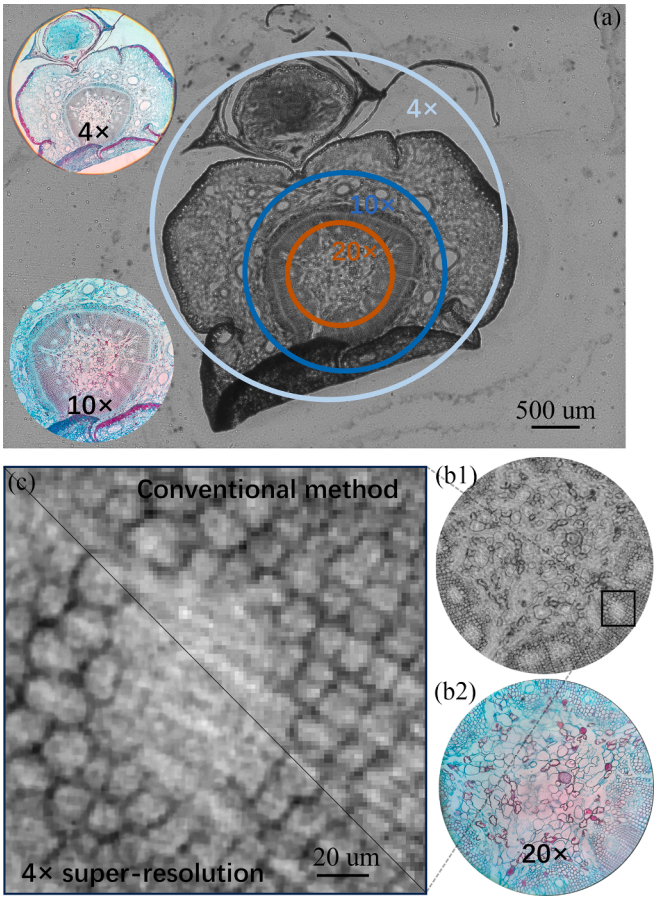

Fig. 6. Reconstruction results of a cross section of pine stems. (a) exhibits the full-field hologram (6.47 × 4.62mm²) with labeled FOV of 4×, 10×, and 20 × microscope objectives from a conventional microscope. (b1) – (b2) show the reconstruction results from the lensless on-chip system and the observation under a 20 × microscope objective for the same area of the section. (c) presents the results of the conventional reconstruction algorithm and the proposed super-resolution reconstruction algorithm based on DAGD.

reaches 2.5 × 10^{-3}, making it still a factor limiting imaging resolution. Smaller emitting chips and narrowband filters may effectively enhance the coherence of the light source. Regarding computational time, the reconstruction algorithms still require substantial computational resources, making real-time reconstruction challenging. In the future, integrating deep learning methods could be explored to improve the efficiency of the reconstruction process.

5. Conclusion

The super-resolution algorithm based on scattering multiplexing and the illumination method using an array light source significantly enhances the imaging resolution of lensless on-chip microscopy systems. The fine modulation of the sample wavefront is achieved at an extremely low cost by applying a scattering layer formed from polystyrene microspheres. Through simulation and experimental validation, we demonstrate the effectiveness of the proposed algorithm in improving resolution. We also analyze the impact of different densities of scattering layer and the number of angles used in array illumination on reconstruction quality, providing guiding suggestions for the practical application of the system. Moreover, the independent update of the scattering layer and the sample effectively suppresses oscillation issues during iteration and greatly improves convergence efficiency. It achieves 1.36 times pixel super-resolution compared with the pixel size of the sensor and reaches the resolution of 1.23 μm under partially coherent light

illumination condition. Additionally, the system requires no calibration process and offers advantages such as compactness and simplicity, providing technical support for low-cost, high-resolution lensless on-chip microscopy systems.

CRediT authorship contribution statement

Yulong Li: Writing – review & editing, Writing – original draft, Software, Methodology, Investigation, Formal analysis, Data curation, Conceptualization. **Zhongrui Lin:** Software, Data curation. **Jianshe Ma:** Supervision. **Chao Zuo:** Writing – review & editing. **Ping Su:** Writing – review & editing, Supervision, Funding acquisition.

Declaration of competing interest

The authors declare the following financial interests/personal relationships which may be considered as potential competing interests: [Ping Su reports financial support was provided by Ministry of Science and Technology of China. If there are other authors, they declare that they have no known competing financial interests or personal relationships that could have appeared to influence the work reported in this paper].

Data availability

Data will be made available on request.

Acknowledgments

This work was supported by the National Key Research and Development program of China (Grant No. 2023YFB3611503), and our authors would like to thank all reviewers for their valuable suggestions.

References

[1] J. Zhang, J. Sun, Q. Chen, et al., Adaptive pixel-super-resolved lensfree in-line digital holography for wide-field on-chip microscopy, Sci. Rep. 7 (2017) 11777, https://doi.org/10.1038/s41598-017-11715-x.
[2] E. Istrate, G. Pedrini, S. Reichelt, Lensless microscopy by multiplane recordings: sub-micrometer, diffraction-limited, wide field-of-view imaging, Opt. Express 31 (2023) 36388–36401, https://doi.org/10.1364/OE.503944.
[3] Y. Huang, M. Zhu, L. Ma, W. Zhang, Accurate and fast registration algorithm for multi-height lensless in-line on-chip holographic microscopy, Opt. Commun. 526 (2023) 128898, https://doi.org/10.1016/j.optcom.2022.128898.
[4] Y. Gao, L. Cao, Projected refractive index framework for multi-wavelength phase retrieval, Opt. Lett. 47 (2022) 5965–5968, https://doi.org/10.1364/OL.476707.
[5] Q. Wang, J. Ma, L. Cao, P. Su, High-resolution portable lens-free on-chip microscopy with RGB LED via pinhole array, Chin. Opt. Lett. 22 (2024) 021101. https://opg.optica.org/col/abstract.cfm?uri=col-22-2-021101.
[6] P. Song, R. Wang, J. Zhu, et al., Super-resolved multispectral lensless microscopy via angle-tilted, wavelength-multiplexed ptychographic modulation, Opt. Lett. 45 (2020) 3486–3489, https://doi.org/10.1364/OL.394923.
[7] C. Zuo, J. Sun, J. Zhang, Y. Hu, Q. Chen, Lensless phase microscopy and diffraction tomography with multi-angle and multi-wavelength illuminations using a LED matrix, Opt. Express 23 (2015) 14314–14328, https://doi.org/10.1364/OE.23.014314.
[8] W. Luo, Y. Zhang, A. Feizi, et al., Pixel super-resolution using wavelength scanning, Light Sci. Appl. 5 (2016) e16060.
[9] W. Luo, A. Greenbaum, Y. Zhang, et al., Synthetic aperture-based on-chip microscopy, Light Sci. Appl. 4 (2015) e261.
[10] Y. Zhou, J. Wu, J. Suo, X. Han, et al., Single-shot lensless imaging via simultaneous multi-angle LED illumination, Opt. Express 26 (2018) 21418–21432, https://doi.org/10.1364/OE.26.021418.
[11] W. Bishara, T. Su, A.F. Coskun, A. Ozcan, Lensfree on-chip microscopy over a wide field-of-view using pixel super-resolution, Opt. Express 18 (2010) 11181–11191, https://doi.org/10.1364/OE.18.011181.
[12] M. Guizar-Sicairos, J.R. Fienup, Phase retrieval with transverse translation diversity: a nonlinear optimization approach, Opt. Express 16 (2008) 7264–7278, https://doi.org/10.1364/OE.16.007264.
[13] G.R. Brady, M. Guizar-Sicairos, J.R. Fienup, Optical wavefront measurement using phase retrieval with transverse translation diversity, Opt. Express 17 (2009) 624–639, https://doi.org/10.1364/OE.17.000624.
[14] W. Bishara, U. Sikora, O. Mudanyali, et al., Holographic pixel super-resolution in portable lensless on-chip microscopy using a fiber-optic array, Lab Chip 11 (7) (2011) 1276–1279, https://doi.org/10.1039/C0LC00684J.
[15] Y. Li, J. Ma, L. Cao, P. Su, Super-resolution lensless on-chip microscopy based on array illumination and sub-pixel shift search, Opt. Lett. 49 (2024) 1620–1623, https://doi.org/10.1364/OL.517347.
[16] S. Zheng, Z. Ding, R. Jiang, C. Guo, Lensless masked imaging with self-calibrated phase retrieval, Opt. Lett. 48 (2023) 3279–3282, https://doi.org/10.1364/OL.492476.
[17] X. Chang, S. Jiang, G. Zheng, L. Bian, Deep distributed optimization for blind diffuser-modulation ptychography, Opt. Lett. 47 (2022) 3015–3018, https://doi.org/10.1364/OL.458434.
[18] Y. Guo, R. Guo, P. Qi, Y. Zhou, Z. Zhang, G. Zheng, J. Zhong, Robust multi-angle structured illumination lensless microscopy via illumination angle calibration, Opt. Lett. 47 (2022) 1847–1850, https://doi.org/10.1364/OL.454892.
[19] C. Lu, Y. Zhou, Y. Guo, S. Jiang, Z. Zhang, G. Zheng, J. Zhong, Mask-modulated lensless imaging via translated structured illumination, Opt. Express 29 (2021) 12491–12501, https://doi.org/10.1364/OE.421228.
[20] M. Pham, A. Rana, J. Miao, S. Osher, Semi-implicit relaxed Douglas-Rachford algorithm (sDR) for ptychography, Opt. Express 27 (2019) 31246–31260, https://doi.org/10.1364/OE.27.031246.
[21] S. Moser, M. Ritsch-Marte, G. Thalhammer, Model-based compensation of pixel crosstalk in liquid crystal spatial light modulators, Opt. Express 27 (2019) 25046–25063, https://doi.org/10.1364/OE.27.025046.
[22] Y. Gao, R. Li, L. Cao, Self-referenced multiple-beam interferometric method for robust phase calibration of spatial light modulator, Opt. Express 27 (2019) 34463–34471, https://doi.org/10.1364/OE.27.034463.
[23] L. Yuanyuan, L. Qingwen, L. You, Z. Junyong, H. Zuyuan, High-resolution multi-planar coherent diffraction imaging with multimode fiber source, Opt. Lasers Eng. 140 (2021) 106530, https://doi.org/10.1016/j.optlaseng.2021.106530.
[24] F. Zhang, B. Chen, G. Morrison, et al., Phase retrieval by coherent modulation imaging, Nat. Commun. 7 (2016) 13367, https://doi.org/10.1038/ncomms13367.
[25] I. Johnson, K. Jefimovs, O. Bunk, et al., Coherent diffractive imaging using phase front modifications, Phys. Rev. Lett. 100 (15) (2008) 155503, https://doi.org/10.1103/PhysRevLett.100.155503.
[26] X. Chang, S. Jiang, Y. Hu, G. Zheng, L. Bian, Pixel super-resolved lensless on-chip sensor with scattering multiplexing, ACS Photonics 10 (7) (2023) 2323–2331, https://doi.org/10.1021/acsphotonics.2c01527.
[27] S. Jiang, P. Song, T. Wang, et al., Spatial- and Fourier-domain ptychography for high-throughput bio-imaging, Nat. Protoc. 18 (2023) 2051–2083, https://doi.org/10.1038/s41596-023-00829-4.
[28] S. Jiang, C. Guo, P. Song, N. Zhou, et al., Resolution-enhanced parallel coded ptychography for high-throughput optical imaging, ACS Photonics 8 (11) (2021) 3261–3271, https://doi.org/10.1021/acsphotonics.1c01085.
[29] A. Maiden, D. Johnson, P. Li, Further improvements to the ptychographical iterative engine, Optica 4 (2017) 736–745, https://doi.org/10.1364/OPTICA.4.000736.
[30] Y. Gao, L. Cao, Generalized optimization framework for pixel super-resolution imaging in digital holography, Opt. Express 29 (2021) 28805–28823, https://doi.org/10.1364/OE.434449.
[31] C. Guo, F.L. Zhang, X.M. Liu, et al., Lensfree auto-focusing imaging using nuclear norm of gradient, Opt. Lasers Eng. 156 (2022) 107076, https://doi.org/10.1016/j.optlaseng.2022.107076.
[32] Y. Huang, S. Jiang, R. Wang, et al., Ptychography-based high-throughput lensless on-chip microscopy via incremental proximal algorithms, Opt. Express 29 (2021) 37892–37906, https://doi.org/10.1364/OE.442530.
[33] A. Ozcan, E. McLeod, Lensless imaging and sensing, Annu. Rev. Biomed. Eng. 18 (2016) 77–102, https://doi.org/10.1146/annurev-bioeng-092515-010849.